IEEE Access
Multidisciplinary : Rapid Review : Open Access Journal

Received 8 June 2023, accepted 20 June 2023, date of publication 26 June 2023, date of current version 20 July 2023.

Digital Object Identifier 10.1109/ACCESS.2023.3289393

RESEARCH ARTICLE

Realization of a Portable Semi-Shielded Chamber for Evaluation of Fat-Intrabody Communication

PRAMOD K. B. RANGAIAH[1], (Member, IEEE), ROGER L. KARLSSON[1], ARVIND SELVAN CHEZHIAN[1], LAYA JOSEPH[1], BAPPADITYA MANDAL[1], (Member, IEEE), BOBINS AUGUSTINE[1,2], (Member, IEEE), MARIA MANI[3], MAURICIO DAVID PEREZ[1], (Member, IEEE), THIEMO VOIGT[2], (Member, IEEE), AND ROBIN AUGUSTINE[1], (Member, IEEE)

[1]Microwaves in Medical Engineering Group, Division of Solid State Electronics, Department of Electrical Engineering, Uppsala University, 751 03 Uppsala, Sweden
[2]Networked Embedded Systems, Department of Electrical Engineering, Uppsala University, 751 03 Uppsala, Sweden
[3]Division of Plastic Surgery, Department of Surgical Sciences, Uppsala University Hospital, 751 85 Uppsala, Sweden

Corresponding authors: Robin Augustine (Robin.Augustine@angstrom.uu.se) and Pramod K. B. Rangaiah (pramod.rangaiah@angstrom.uu.se)

This work was supported in part by the following projects: H2020EU Project (Soft Intelligence Epidermal Communication Platform) under Grant SINTEC-824984, Swedish Foundation for Strategic Research Lifesec: Don't Hack My Body! Project under Grant RIT17-0020, Wireless Brain-Connect inteRfAce TO machineS: B-CRATOS, European Union's Horizon 2020 Research and Innovation Program, Grant agreement ID: 965044, DOI. 10.3030/965044, Funded under EXCELLENT SCIENCE - Future and Emerging Technologies (FET) Open, Coordinated by UPPSALA UNIVERSITET, Sweden. Start date 1 March 2021 and End date 28 February 2025.

ABSTRACT In this work, a customized portable semi-shielded chamber for torso phantoms to evaluate fat-intrabody communication (Fat-IBC) is presented. Fat-IBC is a technology where human fat tissue is used for microwave communication with intrabody medical devices. The potential clinical applications are vast including central nervous system (brain and spine) communication, cardiovascular disease monitoring and metabolic disorder control. However, validating this technology needs assurance that the signal leakage through undesired paths, particularly surface waves and reflections, does not occur. To solve this issue, an effective technique involving a modified design of a semi-shielded chamber is presented. The cross-section of the torso phantoms is about 25 cm × 35 cm and the height about 20 cm. As specified by ISO 3745:2012, the maximum object volume that can be measured in a chamber is 5% of the chamber's internal net volume. Therefore, the dimensions of the semi-shielded chamber was set to 100 cm × 60 cm × 60 cm. The semi-shielded chamber was constructed out of a wooden crate, covered on the inside with microwave absorbers and with thin aluminum sheets on the outside. The experimental evaluation of the semi-shielded chamber was validated according to standards such as EN 50147-1:1996, IEC 61000-4-3:2020, and IEC CISPR 16-1-4:2019. The torso phantom was positioned at the center of the chamber, with a separation wall to ensure signal transmission solely through the phantoms interior and not its surface or chamber walls. The separation wall can be modified either to be conformal to the phantom sample or serve as a solid partition dividing the chamber into two separate volumes for performance measurement. The separation wall was found to have a shielding attenuation of 30 dB to 60 dB for frequencies between 0.7 GHz and 18 GHz, respectively, while the corresponding values for the external walls were found to be 45 dB to 70 dB. The semi-shielded chamber realized in this work is useful for Fat-IBC technology, brain-computer interface, brain-machine interface, body area networks (BANs), and related applications.

INDEX TERMS Anechoic chamber, electromagnetic compatibility, shielding effectiveness measurements, intrabody communication.

The associate editor coordinating the review of this manuscript and approving it for publication was Photos Vryonides.

I. INTRODUCTION

Progress in wireless communication, as well as the most advanced method in electronic devices with highly power-efficient characteristics, have opened up new horizons in human body area networks (BANs) [1]. In human body communication (HBC), multiple devices are worn or placed inside or near the human body. To share data and enable new services, these devices could form a wireless link or a small-scale wireless network [2]. Intrabody communication (IBC) is a wireless communication technique that enables the transmission of data within the human body. It has the potential to revolutionize healthcare and sports technology by providing a reliable and efficient means of transmitting data from inside the body to medical and sports devices. IBC has several advantages over traditional wireless communication techniques, such as higher data rates, lower power, miniaturized transceivers, and greater robustness against interferences and privacy attacks. However, the complex and dynamic nature of the human body presents technical challenges that need to be overcome through continued research and development to realize the full potential of IBC.

Recently, the Fat-IBC technology has got a lot of attention. It has been found that adipose tissue is an effective transmission medium which can serve as a safe and reliable channel for IBC [3]. Basu et al. [4] used the 2.45 GHz Industrial, Scientific, and Medical (ISM) band to demonstrate the use of the fat channel for IBC. EbrahimiZadeh et al. [5], calculated the path loss for Fat-IBC using Poynting vector theory and measured it on ex-vivo porcine fat tissues. Asan et al. [6] characterized the fat channel for IBC at waveguide R-band frequencies (1.7–2.6 GHz). Effects of different fat thicknesses [7], [8] and blood vessel effects have also been studied and compared to the signal coupling [9]. Later, experimental validation of signal path loss for the 5.8 GHz ISM band was performed and the related dynamics of body movements were examined [3]. Furthermore, digital data communication through phantom fat tissue was simulated and measured at 2.0 GHz [10].

A problem for Fat-IBC is that the signals sent between two antennas placed on the skin a distance apart may not be confined to the fat layer only. Parts of the signal may also travel as surface waves along the skin and as free-space waves which can undergo reflections to reach the receiving antenna, so called multipath. In order to eliminate, or at least minimize, the undesired signal paths this study proposes the use of a small anechoic chamber, a semi-shielded chamber, where phantoms emulating different body parts can be placed. Inside the chamber a separation wall, designed to exactly follow the shape of the phantom, will be placed to suppress the undesired signal paths and ensure that the received signal only has travelled through the fat layer.

Since 1953, anechoic chambers [11] are widely used for antenna-related measurements. Anechoic chambers and semi-shielded chambers must satisfy proper boundary conditions to prevent interferences from undesired radiation and reflections [12]. Isolation from undesired sources is achieved by enclosing the chamber with a shielding conductive cover and reflections from the walls are minimized by covering the inside walls with electromagnetic (EM) absorbers [13]. Rectangular-shaped anechoic chambers [14], which are considered here, are suitable for microwaves down to the lowest part of the ultra-high frequency (UHF) band where the reflections from the EM absorbers become non-negligible [15].

Earlier works on anechoic chambers [16], [17], [18] focused on different architectures and measurements such as antenna radiation pattern, gain, and electromagnetic compatibility. However, the purpose of the proposed semi-shielded chamber differs completely from these previous applications. The semi-shielded chamber has been developed to only allow signals to propagate inside phantoms emulating the human torso. Furthermore, the semi-shielded chamber has been evaluated according to all the relevant international standards for measurements in anechoic chambers.

The proposed semi-shielded chamber can be used in the experimental setup for evaluation of offbody, onbody, and inbody communication. It offers a useful setup for Fat-IBC in the areas of brain-computer interface, brain-machine interface, BANs, medical imaging [19], [20], and body sensor networks (BSN), and related applications such as central nervous system (brain and spine) communication, cardiovascular disease monitoring, and metabolic disorder control (diabetes, obesity etc).

This paper is organized in the following way. In Section II the problems and solutions of conducting Fat-IBC experiments in an anechoic chamber are discussed. An explanation of the simulation and construction of the semi-shielded chamber is presented in Section III. Experimental validation of the chamber based on relevant standards and a discussion on suppressing surface waves are addressed in Section IV. In Section V the impact of the separation wall is quantified for a torso phantom. Section VI concludes the paper.

II. PROBLEMS AND METHODOLOGY

In this section, an appropriate way to measure Fat-IBC inside a semi-shielded chamber for torso phantoms is outlined. Fat-IBC onbody antennas [21] are placedÂ onÂ a torso phantom with multiple layers, representing skin, fat, muscle, internal organs, and bone. The Fat-IBC antennas match the impedance of the skin layer, resulting in better electric field coupling into the underlying fat layer. It has been shown that signals are less attenuated in fat tissue than in muscle tissue [6]. Signal transmission through muscle is inefficient due to high dielectric losses ($\tan\delta_e = (\omega\epsilon'' + \sigma)/\omega\epsilon'$ [22]) and the attenuation per length unit in muscle tissue is more than twice as high as in fat tissue [6].

A. PROBLEM

The signals sent between two Fat-IBC antennas placed on a phantom will propagate through the emulated fat tissue, but a part may propagate as surface waves along the skin of the phantom and another part may leak out and reflect against the inside walls of the chamber and finally reach the receiving

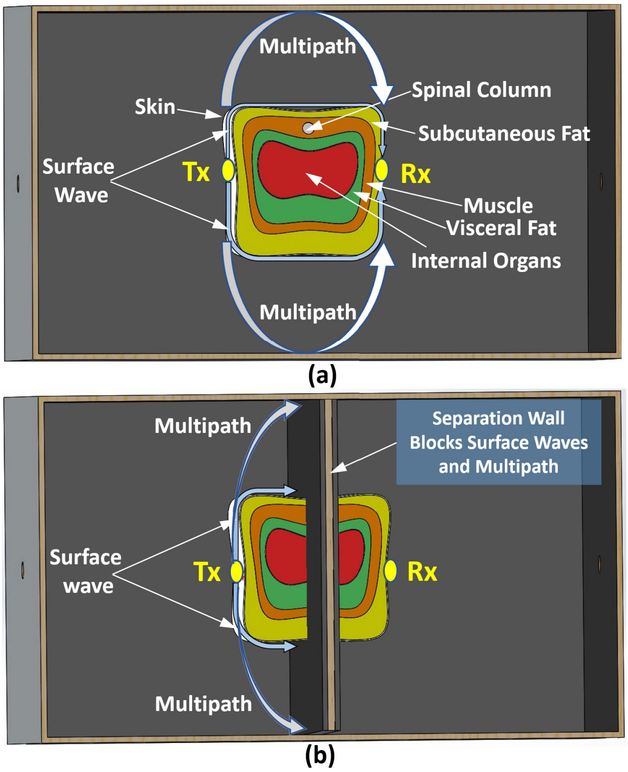

FIGURE 1. The proposed Fat-IBC technique, (a) problem posed by external signal paths such as surface waves and multipath, and (b) surface wave suppression by introducing a septum wall a cross the phantom.

antenna, so called multipath. Figure 1(a) illustrates the Fat-IBC measurement problem with external paths like surface waves and multipath.

B. SOLUTION

The problem with the two external propagation paths can be solved by introducing a separation wall inside the semi-shielded chamber, see Figure 1(b). The separation wall is placed in the middle of the chamber and is shaped according to the geometry of the phantom with absorber material in contact with the phantom to eliminate the surface waves. Furthermore, the separation wall blocks multipath by preventing wall reflections from travelling into the other part of the chamber. In this way the signal can only propagate through the fat layer to reach the receiving antenna and an effective free space test setup for Fat-IBC is formed.

III. DESIGN AND DEVELOPMENT OF SEMI-SHIELDED CHAMBER FOR TORSO PHANTOMS

In this section, the design and development of the semi-shielded chamber for torso phantoms is presented. A computer simulation of the semi-shielded chamber is provided and the efficiency of the chamber is discussed.

Anechoic chambers range from small compartments the size of household microwave ovens to sizes as large as aircraft hangars. The size of the chamber depends on the size of the test object and the frequency range. The standard ISO 3745:2012 [23], regulates the anechoic chamber dimensions based on the volume of the test object, as given by the volumetric relation

$$V_{\text{object}} \leq 0.05\, V_{\text{chamber}} \tag{1}$$

where V_{object} is the net volume of the object to be measured, i.e. the torso phantom volume, and V_{chamber} is the net volume of the semi-shielded chamber. The torso phantoms to be measured have lengths between 20 cm and 40 cm and, to allow for space to place the Fat-IBC antennas on the phantom, the length of the chamber was set to 100 cm. The height of the torso phantoms, about 20 cm, set the height of the chamber to 60 cm. There were no requirements on the width of the chamber and a quadratic cross section was chosen with width 60 cm. This gives a chamber of size $V_{\text{chamber}} = 100\text{ cm} \times 60\text{ cm} \times 60\text{ cm} = 0.36\text{ m}^3$ and, according to Equation (1), a maximum phantom volume, V_{object}, of 0.018 m^3.

A. SIMULATION USING COMSOL MULTIPHYSICS

COMSOL Multiphysics provides several inbuilt models related to anechoic chambers [24] which makes simulations quick and accurate. Even though the semi-shielded chamber is covered with flat absorbers inside, the provided simulation model involves pyramidal-shaped absorbers and therefore the simulation was performed in this way. Inside the simulated chamber, absorbers were configured on all the surfaces in the form of an array of pyramidal structures. The pyramidal shape forces the incident waves to undergo multiple energy-reducing reflections until they reach the base of the pyramidal array with substantially lower field amplitudes, giving minimal scattering back from the walls. By absorbing electromagnetic waves inside the chamber and blocking outside signals, the chamber creates a virtually infinite space that has almost no internal reflections and does not suffer from any undesired external RF noise [24].

Figure 2(a) shows the anechoic chamber simulation model. The model consists of three layers which are, from inside to outside: microwave absorber, a 0.85 cm thick wooden structure, and a 30 μm aluminum layer. Figure 2(b) presents a wire-frame rendering view of the anechoic chamber including absorbers based on the inbuilt models of COMSOL with an array of pyramidal objects. Foley [25], discusses in detail the radiation absorbent material used in the simulation, a low conductive material with conductivity $\sigma = 0.5$ S/m and $\epsilon_r = \mu_r = 1$.

For the simulation, a dipole antenna [26] resonant at 2.45 GHz was used. In Figure 2(c) its resonant torus-shaped 3D far-field power pattern is displayed. The electric field of the dipole antenna was simulated inside the chamber and in Figure 2(d) the radiated power inside the anechoic chamber is plotted showing that the field is weakest at the walls where the absorbers are situated.

The semi-shielded chamber makes a suitable environment for accurately measuring the performance of wireless devices and antennas, free from external interference. However, apart from the simulation it is also necessary to validate that the

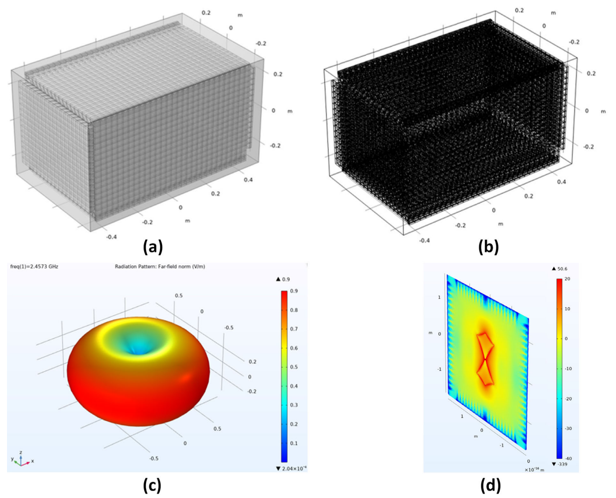

FIGURE 2. **The performance of the 100 cm × 60 cm × 60 cm large semi-shielded chamber was simulated with COMSOL Multiphysics. Pyramidal-shaped EM absorbers, the wooden structure, and the conducting aluminum sheet were all included in the simulation model. Panel (a) view with closed mesh transparency; (b) wire-frame rendering view; (c) 3D far-field pattern of a dipole antenna at 2.45 GHz placed inside the chamber; and (d) electric field simulation with a dipole antenna inside the chamber.**

semi-shielded chamber conforms to the established standards for anechoic chambers required to make it suitable for testing wireless devices and antennas. This is done in the next section.

B. CONSTRUCTION OF THE SEMI-SHIELDED CHAMBER FOR TORSO PHANTOMS

Here, the construction of the semi-shielded chamber for torso phantoms is discussed. As previously mentioned, a wooden crate of size 100 cm × 60 cm × 60 cm and 0.85 cm thickness was chosen. Inside the crate, microwave absorbing material of type EA-LF500-24 [27] was pasted. This is a dielectrically loaded carbon polyurethane foam with insertion loss varying from 20 dB to 34 dB for frequencies of 700 MHz and 18 GHz, respectively. The outside of the box was covered with a 30 μm thick aluminum layer, which prevents EM waves from leaking out of the chamber and external EM waves from entering the chamber. Figure 3(a) shows a photograph of the implemented semi-shielded chamber. At critical places along the seams between the side surfaces and at the bottom plane, multiple layers of aluminum have been used to ensure that no leakage take place. The bottom of the chamber has 6 legs and every leg has a wheel attached to make the chamber portable. Figure 3(b) shows how the lid, or top wall, can be opened to allow torso phantoms and other devices to be placed inside the chamber. Small holes for RF-cables have been made on the two short sides. The gap between the cable and the orifice was pasted with shield material to minimize leakage.

1) PENETRATION DEPTH OF EM WAVES INTO AN ALUMINUM SHEET

The shield efficiency of the 30 μm aluminum sheet needs to be evaluated. The penetration depth of microwaves inside

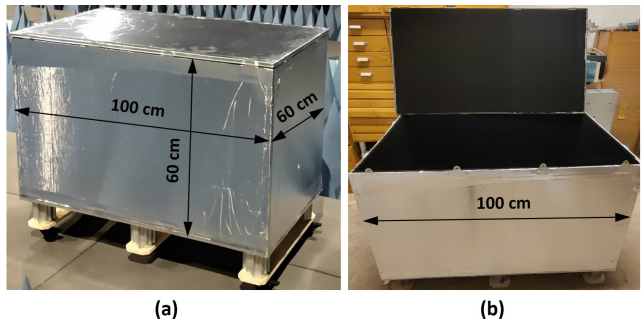

FIGURE 3. **Photographs of the semi-shielded chamber, (a) outside and (b) with the lid (top wall) opened.**

a good conductor, like a metal, is characterized by the skin depth δ_s [22]

$$\delta_s = \sqrt{\frac{2}{\omega\mu\sigma}} \tag{2}$$

where $\omega = 2\pi f$ is the angular frequency in radians/s, μ the magnetic permeability in H/m, and σ the conductivity in S/m. For aluminum we can set $\mu = \mu_0 = 4\pi \times 10^{-7}$ H/m and the conductivity has the value $\sigma = 3.77 \times 10^7$ S/m.

The skin depth is the distance inside the material where the field has decayed to $1/e$ ($= 36.8\%$) of its value at the surface. For example, at the depth of $6\delta_s$ the field has decayed to 0.25% of the value at the surface, or decayed by 52.1 dB. For the lowest and highest frequencies used in this paper, 700 MHz and 18 GHz, the skin depths become 3.1 μm and 0.61 μm, respectively. In the worst case of the lowest frequency, the 30 μm thick aluminum sheet represents about $10\delta_s$ and an attenuation of almost 87 dB. This value is sufficient for the semi-shielded chamber.

C. ANTHROPOMORPHIC OBESE TORSO PHANTOM

Figure 4 shows an anthropomorphic obese torso phantom of the human abdominal region. This phantom, which has been developed for Fat-IBC, consists of tissues like skin, subcutaneous fat, muscle, spinal column, visceral fat, and internal organs. The thicknesses of the tissues have been chosen according to the average thicknesses of the obese human body [28]. The torso phantom has length 25.2 cm, width 24.5 cm, and height 18.5 cm. The main constituents of the torso phantom and the fabrication procedure of each tissue are described by Joseph et al. [29]. By utilizing the semi-shielded chamber signals can only propagate through the subcutaneous fat layer.

D. MODIFICATION OF THE CHAMBER SEPARATION WALL

In order for the separation wall to block surface waves along the skin of the phantom, it has to be modified according to the shape of the phantom. The separation wall is made of the same 0.85 cm thick wooden structure and is covered on both sides with absorbers. The torso abdominal torso phantoms are all almost 20 cm tall and to simplify the setup inside the

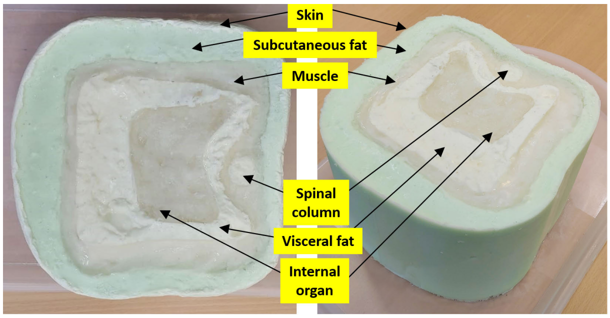

FIGURE 4. **Obese abdomen torso phantom with the emulated tissues indicated, (a) top view and (b) oblique view.**

chamber, the 60 cm high separation wall has been divided into two parts, an upper part of 40 cm and a 20 cm lower part. In this way the upper part of the separation wall can remain the same for all the measurements while only the lower part needs to be modified according to the shape, size, and position of the torso phantom.

For the measurements the obese torso phantom was placed at the middle of the semi-shielded chamber. Two phantom orientations were considered: with the spinal column placed vertically along the separation wall for side-to-side measurements and with the spinal column still vertical but rotated 90 degrees for front-to-back measurements. The dimensions across the phantom are marginally the same for front-to-back and side-to-side. Figure 5 displays three views of how the separation wall has been adapted to the torso phantom. Figure 5(a) shows an oblique view where the separation wall can be seen to be kept in place by plastic clamps mounted with plastic screws on the middle of the long sides of the chamber. Figures 5(b) and (c) shows a side view and a top view, respectively. The side view shows that the lower part of the separation wall has been modified according to the geometry of the torso phantom, thereby not only eliminating surface waves but also preventing reflections from reaching the other side of the chamber.

IV. EXPERIMENTAL VALIDATION OF THE CHAMBER

In this section, the experimental validation of the semi-shielded chamber is described. The process involves three separate aspects for the chamber: shield attenuation, field uniformity, and site voltage standing wave ratio (VSWR). In the following, these three validation measurements are described.

A. SHIELD ATTENUATION MEASUREMENT

The EN50147-1:1996 standard [30] describes how shield attenuation measurements of shielded enclosures should be performed in the frequency range 9 kHz to 40 GHz. For the semi-shielded chamber the procedure outlined in the standard has been followed using a pair of horn antennas in the frequency range 700 MHz to 18 GHz and a pair of stubby monopole antennas for 700 MHz to 2.7 GHz.

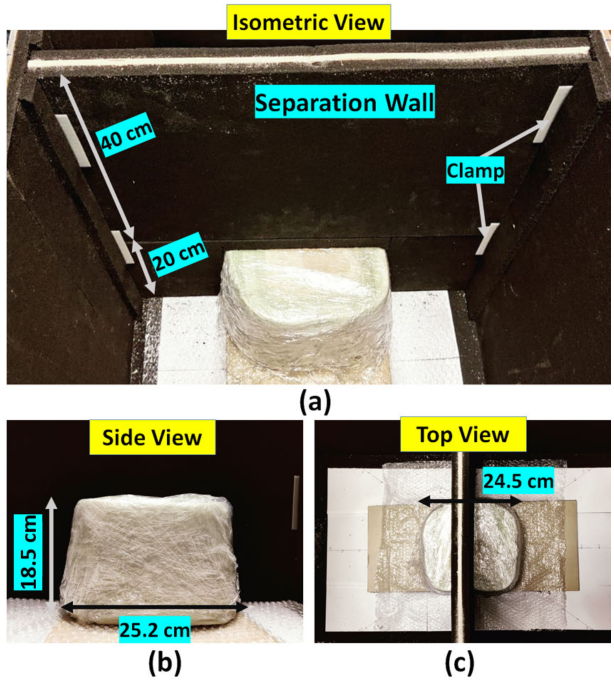

FIGURE 5. **Customized separation wall for the obese torso phantom. Panel (a) shows how the separation wall has been divided into an upper unabbreviated part and a lower modified part and how it is held into place with clamps, (b) side view, and (c) top view.**

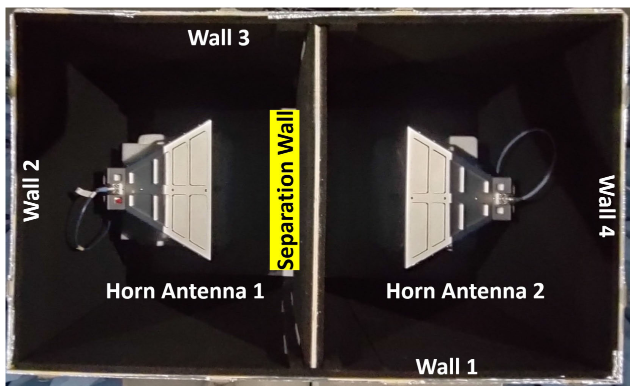

FIGURE 6. **Semi-shielded chamber with horn antennas to measure the shield attenuation of the separation wall.**

1) SHIELD ATTENUATION MEASUREMENTS WITH HORN ANTENNAS

Shield attenuation measurements were performed in the frequency range 700 MHz to 18 GHz using two double ridged broadband waveguide horn antennas, HA-07M18G-NF [31].

In order to evaluate the shield efficiency of the separation wall, the experimental setup of Figure 6 was used. The horn antennas were placed 40 cm apart (aperture to aperture), at the same height, and aligned towards each other with the same polarization. The semi-shielded chamber was closed and the RF cables to the antennas were routed through two orifices on the opposite short sides of the chamber, one cable per orifice. Pieces of adhesive microwave shielding sheets were

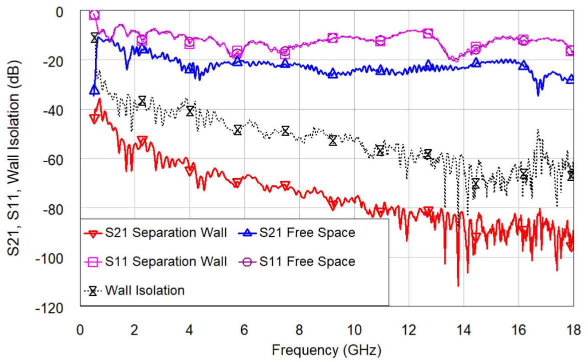

FIGURE 7. Shield attenuation of the separation wall measured with two horn antennas placed on either sides of the separation wall 40 cm apart.

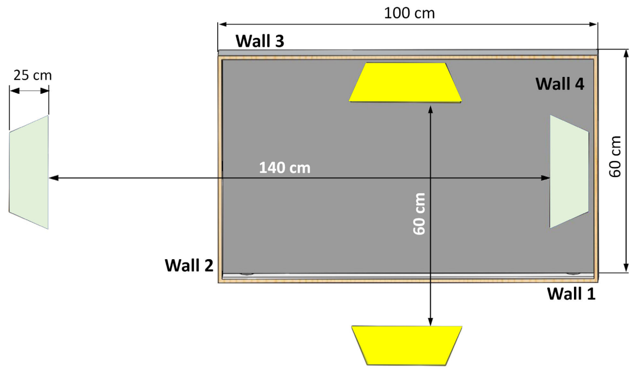

FIGURE 8. Measurement setup for shield attenuation measurements for Walls 1 and 2 using horn antennas.

used to cover the gaps between the orifices and the cables. The RF cables were connected to a N9918A FieldFox vector network analyzer (VNA), which measured the scattering parameters S21 and S11, where the transmission parameter S21 is the most interesting, indicating the power transmitted from antenna 1 to antenna 2.

Figure 7 shows the results of the shield measurements of the separation wall. The red curve with downward facing triangles shows the transmission measurement, S21, of the separation wall and the blue curve with upward facing triangles shows the corresponding measurement of the free space attenuation (without separation wall) with the horn antennas placed inside a standard ETS-Lindgren anechoic chamber [32]. The difference between the red curve and the blue curve is the shield attenuation of the separation wall (wall isolation), shown in Figure 7 as the dashed black curve with both upward and downward facing triangles combined. It can be seen that the separation wall provides at least 30 dB attenuation and for frequencies higher than 4 GHz the attenuation is more than 40 dB and increases to 60 dB at 14 GHz. Figure 7 also shows reflection measurements, S11, both in the presence of the separation wall, pink curve with squares, and for the free space measurement in the ETS Lindgren chamber, purple curve with circles. The two S11 curves are almost identical and difficult to separate in the figure.

The outer walls of the semi-shielded chamber should provide similar values for the shield attenuation as the separation wall, i.e. between 40 dB and 60 dB. Figure 8 shows a top view of the setups for measuring the shield attenuation of Walls 1 and 2. The setups for measuring Walls 3 and 4 are similar but the positions of the antennas are mirrored with respect to the two orthogonal central symmetry lines of the chamber. For the Walls 1 and 3 the horn antennas were placed 60 cm apart (aperture to aperture) with the transmitting horn antenna inside the semi-shielded chamber and the receiving antenna outside the chamber. For Walls 2 and 4 the distance between the antenna apertures was 140 cm. Free space measurements were also made with the horn antennas separated by the same distances of 60 cm and 140 cm in a standard ETS-Lindgren anechoic chamber [32].

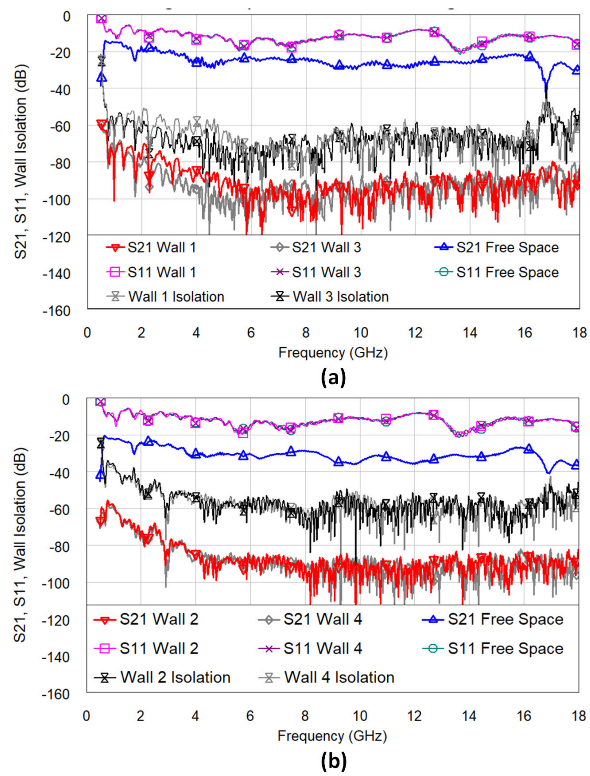

FIGURE 9. Shield attenuation of (a) the large Walls 1 and 3 for 60 cm separation between the horn antennas, (b) the small Walls 2 and 4 with 140 cm separation between the horn antennas.

Figure 9(a) shows the result of the shield attenuation measurements of the largest outer Walls 1 and 3. The two curves at the bottom show the transmission measurements, S21, of Wall 1 (red with downward facing triangles) and Wall 3 (grey with diamonds). The free space S21 measurement is shown as the blue curve with upward facing triangles. The difference between the wall attenuation and the free space attenuation is the shield attenuation of Walls 1 and 3, grey and black curves, respectively, both with double triangles. It can be seen that Walls 1 and 3 provide shield attenuation of about 60 dB over the whole frequency range from 700 MHz

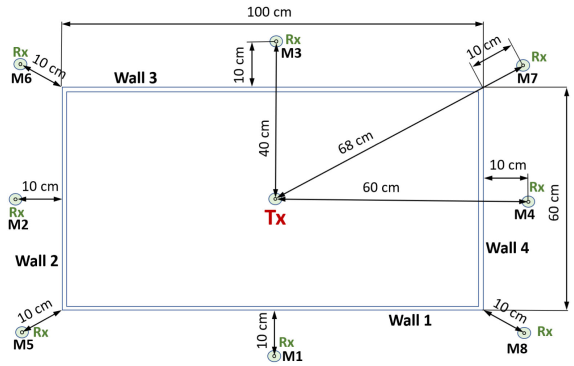

FIGURE 10. Setup for shield attenuation measurements with Mike 1C antennas.

to 18 GHz. The reflections, S11, pink and purple for the two walls and light blue for free-space, are practically identical.

For Walls 2 and 4, the results are presented in Figure 9(b) with the same line styles and colors as in Figure 9(a). For these two short side walls the shield attenuation is slightly better than 50 dB for the whole frequency range which is less than for the larger walls. Two reasons can potentially explain the lower wall attenuation. The first can be leakage through the cable orifices on the short side Walls 2 and 4. The second cause can be leakage from the edges of the chamber. For the small side Walls 2 and 4, the edges are closer to the direct line of sight between the antennas than for the larger Walls 1 and 3 and this may contribute to a smaller shield attenuation.

2) SHIELD ATTENUATION MEASUREMENT WITH MIKE 1C ANTENNAS

The Mike 1C antenna [33] is a commercially available vertically polarized monopole antenna for frequencies between 700 MHz and 2 700 MHz (for 960 MHz–1 700 MHz VSWR < 2.0). Since the semi-shielded chamber mainly will be used for Fat-IBC with WLAN, Bluetooth, and Zigbee protocols, which all have frequency bands covered by the Mike 1C antenna, this antenna has been used to test the shield attenuation of the outer walls and to examine any potential leaks at the edges of the chamber. Figure 10 shows the setup for shield attenuation measurement using a pair of Mike 1C antennas. The transmitting antenna (Tx) was placed at the middle of the chamber, elevated 25 cm from the bottom. Measurements were taken at eight positions (M1–M8) outside the chamber with the receiving antenna (Rx) placed 10 cm from the chamber at the same height as the transmitting antenna. The eight positions include all mid points of the four outer walls and all four vertical edges. Comparative measurements were made in terms of free space measurements at the same distances (40, 60, and 68 cm) in a standard ETS-Lindgren anechoic chamber [32].

Figure 11 shows the result of the shield attenuation measurement using Mike 1C antennas. The line styles and colors are the same as in Figure 9. Figure 11(a) displays S21 for the M1 and M3 points (Walls 1 and 3). The distance between

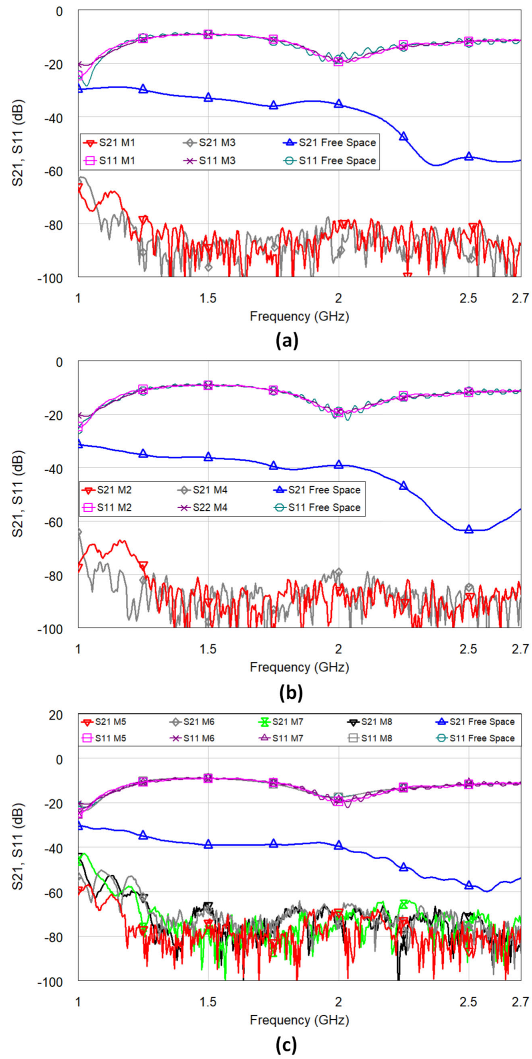

FIGURE 11. Result of the shield attenuation measurements using Mike 1C stubby antennas for positions (a) M1 and M3, (b) M2 and M4, and (c) M5, M6, M7, and M8.

the antennas is 40 cm and the results are compared with free space measurement in a standard ETS-Lindgren anechoic chamber [32]. Walls 1 and 3 offer at least 50 dB attenuation up to 2.15 GHz, which is similar to the results with the horn antennas shown in Figure 9(a). Figure 11(b) shows the S21 measurements for the M2 and M4 points, corresponding to the smaller Walls 2 and 4, respectively, and a spacing of 60 cm between the antennas. Again, the attenuation values are similar to the values measured with horn antennas, see Figure 9(b). Figure 11(c) illustrates the S21 measurements for the vertical edges (the points M5, M6, M7, and M8), where the antennas were separated by a distance of 68 cm. An attenuation of at least 40 dB can be found at each vertical edge.

B. FIELD UNIFORMITY

Measeurements of field uniformity of an anechoic chamber should be performed according to the standard IEC61000-4-3:2020 [34]. The purpose is to verify that the electric field

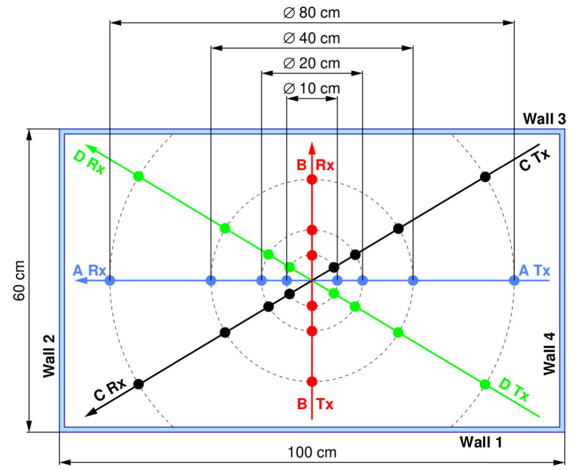

FIGURE 12. Field uniformity measurement plan with grid points for the S21 measurements.

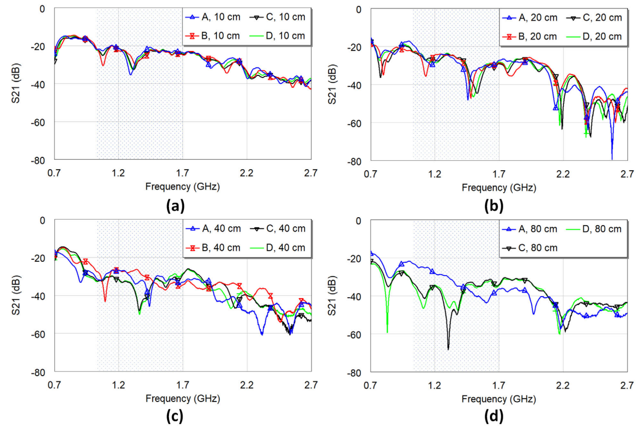

FIGURE 13. S21 measurements to check the field uniformity inside the semi-shielded chamber at distances of (a) 10 cm, (b) 20 cm, (c) 40 cm, and (d) 80 cm.

inside the anechoic chamber is uniform across the test area where measurements will take place. Since the semi-shielded chamber is small compared to a standard chamber, only 100 cm × 60 cm × 60 cm, and that the torso phantoms will be placed at the middle of the chamber, the test points have been chosen to be positioned more densely at the middle of the chamber as shown in Figure 12. More specifically, the test points have been chosen as the intersections between four circles of diameters 10, 20, 40, and 80 cm, and four straight lines, where two of the lines connects the midpoints of the vertical sides (lines A and B) and the other two lines connect the opposite edges (lines C and D) of the semi-shielded chamber. For each measurement the transmitting antenna was placed at a specific test point and the receiving antenna was placed at the opposite test point on the same circle which intersects the same line as the first test point. In this way, four measurements at different distances were made for each of the radial lines A, C, and D. For line B, the test point at the 80 cm diameter circle falls outside the semi-shielded chamber and only three measurements were made.

Figure 13 shows the result of the field uniformity measurement where S21 was measured along the lines A, B, C, and D at distances of (a) 10 cm, (b) 20 cm, (c) 40 cm, and (d) 80 cm. According to the IEC 61000-4-3:2020 standard [34], field variations for different measurement directions of up to 6 dB are acceptable for practical test conditions.

For the close range measurements at 10 cm and 20 cm in Figures 13(a) and (b), respectively, which cover a very important test area for Fat-IBC measurements, all the measurement curves are very similar indicating an excellent field uniformity. Even though, slight variations may occur because of errors in the antenna placement positions and even smaller variations may arise due to the pre-distorted cables of the Mike 1C antennas which piece-wise may be aligned with the vertically polarized Mike 1C antennas.

In case of the long range measurements at 40 cm and 80 cm distance shown in Figure 13(c) and (d), respectively, the antennas are closer to the walls of the chamber and reflections come into play. The absorbers [27] at the inside chamber walls offer an insertion loss of at least 20 dB, which may not be negligible. On the other hand, with increasing distance between the antennas the placement errors become less important.

The 40 cm distance measurement at the middle of the short sides of the chamber, along line B, red curve in Figure 13(c), suffers from higher reflections than the other measurements at the same distance. Depending on the phase of the reflected wave the reflections can be either constructive or destructive giving rise to higher and lower magnitude of S21, respectively. In Figure 13(c), this is illustrated by the fact that the measurement along line B (red curve) have a tendency to have either the highest or the lowest value of S21. For line A, blue curve in Figure 13(c), reflections may also be contributing, but due to the larger distance to the reflecting walls, about 30 cm, the reflections are weaker and the fluctuation of S21 is less than for measurements along line B. The diagonal of the chamber, lines C and D, are symmetric and these measurements show a striking similarity. Due to multiple reflections at the edges of the chamber, both attenuating the signals and spreading them in favorable directions, the reflections are minimal.

The measurements at 80 cm distance shown in Figure 13(d) for the lines A, C, and D, display similar characteristics as the measurement at 40 cm distance, but even more pronounced. For line A the antennas are placed only about 10 cm from the walls of the chamber and reflections from the flat absorber surfaces contribute in a similar way as for line B for the 40 cm diameter case, showing both constructive and destructive interference making the measured S21 values either higher or lower that the values for the diagonal lines C and D. For the diagonal lines C and D, the situation is similar to the corresponding 40 cm case with multiple reflections attenuating and scattering the signals, and the measured curves are very similar.

C. SITE VOLTAGE STANDING WAVE RATIO (VSWR)

For an anechoic chamber or open area test site, site VSWR characterizes the suitability for radiation emission tests [35].

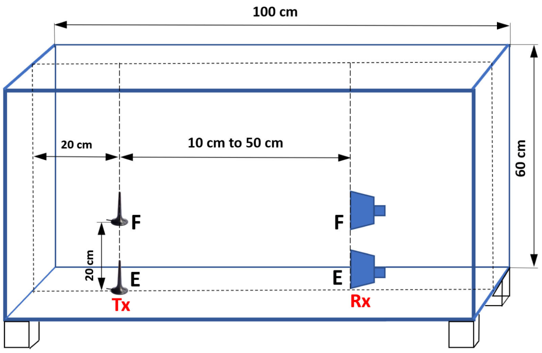

FIGURE 14. Setup for site VSWR measurement. Two heights (E and F) have been evaluated.

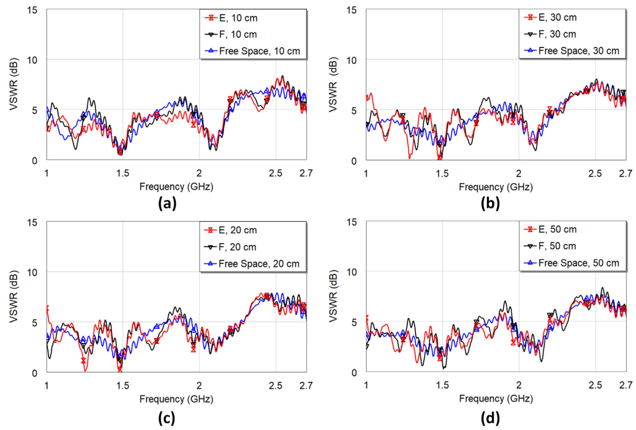

FIGURE 15. Results of site VSWR measurements for heights E and F inside the semi-shielded chamber and for free space. The distances between the antennas are (a) 10 cm, (b) 20 cm, (c) 30 cm, and (d) 50 cm.

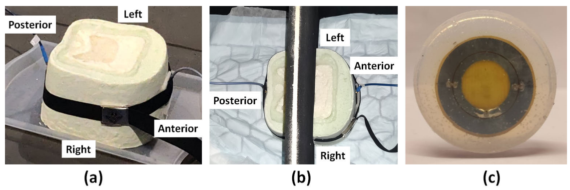

FIGURE 16. Setup to analyze the impact of a separation wall on an obese torso phantom equipped with ring-shaped Fat-IBC antennas, (a) the torso phantom without the separation wall, (b) the torso phantom with the separation wall, and (c) the ring-shaped Fat-IBC antenna used in the measurements.

Site VSWR is very important for frequencies above 1 GHz. Below 1 GHz, normalized site attenuation is sufficient for chamber authentication. For site VSWR tests, the standard IEC CISPR 16-1-4:2019 [36] has been followed. This standard prescribes that the site VSWR must be evaluated with the receiving antenna and for that purpose a double ridge guide horn antenna, SAS-571 [37], covering the frequency range 700 MHz to 18 GHz, has been used. This antenna has high gain and low VSWR and is an excellent choice for both immunity and emission testing. For transmission, a vertically polarized Mike 1C antenna [33] has been used.

Figure 14 shows the site VSWR measurement setup. The transmitting Mike 1C antenna was placed 20 cm from the short-side wall where it is outside of the region where the torso phantom will be placed. The receiving horn antenna was placed in the region for the torso phantom at a distance ranging from 10 cm to 50 cm from the transmitting antenna. Two different heights, marked with letters E and F, were evaluated. Height E is for the bottom of the chamber where the torso phantom is placed. Height F corresponds to the upper height of the torso phantom 20 cm above the bottom of the chamber. In both cases, E and F, the height of the receiving horn antenna was adjusted to coincide with the height of the transmitting antenna.

In Figure 15 the measured VSWR of the receiving horn antenna is plotted for heights E and F at distances of (a) 10 cm, (b) 20 cm, (c) 30 cm, and (d) 50 cm. The results are also compared with free space measurements at the same distances in a standard ETS-Lindgren anechoic chamber [32]. All the VSWR measurements, regardless of distances and positions, are within acceptable values (less than 10).

The successful results of the three tests presented in this section implies that the semi-shielded chamber is performing sufficiently well to function as a substitute for a standard anechoic chamber. Therefore, the proposed chamber can be used for evaluating Fat-IBC.

V. EVALUATING THE SEMI-SHIELDED CHAMBER FOR FAT-IBC

During quantification of signal propagation through subcutaneous fat tissue (fat channel) all the alternative propagation paths, like surface waves and multipath, have to be suppressed. In this section the capacity of the semi-shielded chamber to suppress surface waves and multipath is demonstrated with measurement results. In Figure 16(a) the basic measurement setup for a torso phantom without separation wall is shown. This setup is similar to the problematic setup identified in Figure 1(a). In Section II-B an improved setup with a separation wall across the torso phantom was discussed and this setup is shown in Figure 16(b). The obese torso phantom has been placed at the middle of the chamber and the separation wall can be seen to divide the chamber into two equal parts with half of the phantom in each part. Measurements were taken in two directions: anterior-posterior (front-to-back) and mediolateral (side-to-side) in both left and right lateral positions. Two customized circular antennas [38] were used in the measurement setup, see Figure 16(c), and this antenna type has been optimized to resonate at 2.45 GHz when placed on human skin. The antenna is a vertically polarized dual loop designed to couple microwave signals through the skin and into the human fat layer. The two antennas were held in place on the torso phantom by a polystyrene belt which can be seen in Figure 16(a) and (b).

The measured scattering parameters S21, S11, and S22 are shown in Figure 17, with and without separation wall. Panel (a) shows the front-to-back measurements and Panel (b) the side-to-side measurements. Without the separation wall the signal transmission S21 (red curves in Panels (a) and (b)) is high for both torso positions due to additional propagation possibilities in terms of surface waves and multipath.

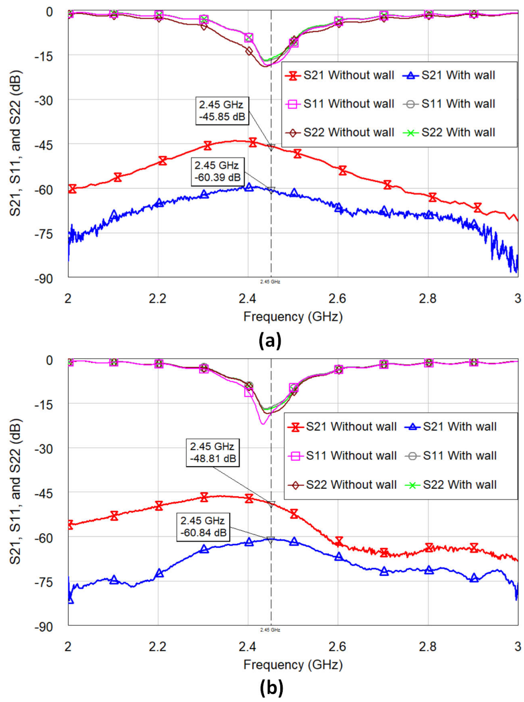

FIGURE 17. **Comparison of scattering parameters S21, S11, and S22 measured on a torso phantom with and without separation wall for (a) front-to-back and (b) side-to-side measurements. The S21 parameter indicates a substantial difference in transmission between the two cases.**

With the separation wall in place, S21 (blue curves) drop significantly when the signal only can propagate through the fat channel For front-to-back measurements the difference made by the separation wall at 2.45 GHz is 14.5 dB. On average between 2 GHz and 3 GHz the difference is 13 dB. For side-to-side measurements, the difference is 12 dB at 2.45 GHz with an average of 12.5 dB over the displayed frequency band. These measurements show that the semi-shielded chamber equipped with a separation wall substantially reduces surface waves and multipath making it to a viable experimental setup for Fat-IBC.

VI. CONCLUSION

In this paper a customized design of a portable semi-shielded chamber for evaluation of Fat-IBC measurement setups is presented. Any anechoic chamber can eliminate interfering microwave signals, but the challenges are surface waves and multipath propagation. In order to eliminate surface waves and multipath a separation wall conforming to the shape of the torso phantom was developed. The semi-shielded chamber was designed to house phantoms of various human body parts and in particular torso phantoms with diameters of 25 cm to 35 cm. According to the standard ISO 3745:2012, the maximum object volume that can be measured in a chamber is 5% of the internal net volume of the chamber. Therefore, the semi-shielded chamber was designed with a size of 100 cm × 60 cm × 60 cm. Further verification of the customized dimensions was made by a simulation with COMSOL Multiphysics using the electric field from a dipole antenna inside. The semi-shielded chamber was constructed from a wooden crate covered on the inside with microwave absorbers and on the outside with aluminum sheets. In order to assess the EMC and radio disturbance characteristics, the semi-shielded chamber was evaluated against the standards EN 50147-1:1996 for shield attenuation, IEC 61000-4-3:2020 for field uniformity, and IEC CISPR 16-1-4:2019 for site VSWR. Horn antennas of type HA-07M18G-NF with high gain have been used for shield attenuation measurements and another horn antenna, of type SAS-571, with low VSWR was used to measure site VSWR. These antennas are excellent choices for both immunity and emission testing. Mike 1C antennas have also been used and they are suitable for testing the performance of the walls and edges of the chamber. The shield efficiencies of the separation wall and all outer walls were measured, yielding shielding values ranging from 40 dB to 70 dB for the frequencies 0.7 GHz and 18 GHz, respectively and confirming that the shielding efficiency of the semi-shielded chamber is sufficient. Comparisons have also been made with a standard ETS-Lindgren anechoic chamber with results which are promising for use in Fat-IBC experiments.

Fat-IBC experiments have been performed in the semi-shielded chamber with and without separation wall, giving a difference of 13 dB and 12.5 dB for front-to-back and side-to-side measurements, respectively. This is because of elimination of external signals and that the separation wall blocks surface waves and multipath propagation. The chamber was constructed as a fundamental part of the experimental setup for Fat-IBC-based microwave experiments on torso phantoms. These experiments will improve the understanding and applicability of Fat-IBC based communication in humans and guide future clinical applications.

REFERENCES

[1] A. Moin, A. Thielens, A. Araujo, A. Sangiovanni-Vincentelli, and J. M. Rabaey, "Adaptive body area networks using kinematics and biosignals," *IEEE J. Biomed. Health Informat.*, vol. 25, no. 3, pp. 623–633, Mar. 2021.

[2] R. Cavallari, F. Martelli, R. Rosini, C. Buratti, and R. Verdone, "A survey on wireless body area networks: Technologies and design challenges," *IEEE Commun. Surveys Tuts.*, vol. 16, no. 3, pp. 1635–1657, 3rd Quart., 2014.

[3] N. B. Asan, E. Hassan, M. D. Perez, L. Joseph, M. Berggren, T. Voigt, and R. Augustine, "Fat-intrabody communication at 5.8 GHz: Verification of dynamic body movement effects using computer simulation and experiments," *IEEE Access*, vol. 9, pp. 48429–48445, 2021.

[4] S. Basu, D. Mitra, B. Mandal, and R. Augustine, "Antenna based RF techniques for intrabody communication," in *IEEE MTT-S Int. Microw. Symp. Dig.*, Dec. 2020, pp. 1–4.

[5] J. EbrahimiZadeh, S. A. A. Jahromi, M. D. Perez, and R. Augustine, "Pathloss calculation for fat-intra body communication using Poynting vector theory," in *Proc. 14th Eur. Conf. Antennas Propag. (EuCAP)*, Mar. 2020, pp. 1–5.

[6] N. B. Asan, E. Hassan, J. Velander, S. R. Mohd Shah, D. Noreland, T. J. Blokhuis, E. Wadbro, M. Berggren, T. Voigt, and R. Augustine, "Characterization of the fat channel for intra-body communication at R-band frequencies," *Sensors*, vol. 18, no. 9, pp. 2752–2768, 2018.

[7] N. B. Asan, D. Noreland, E. Hassan, S. R. M. Shah, A. Rydberg, T. J. Blokhuis, P. Carlsson, T. Voigt, and R. Augustine, "Intra-body microwave communication through adipose tissue," *Healthcare Technol. Lett.*, vol. 4, no. 4, pp. 115–121, Aug. 2017.

[8] N. B. Asan, J. Velander, S. Redzwan, M. Perez, E. Hassan, T. J. Blokhuis, T. Voigt, and R. Augustine, "Effect of thickness inhomogeneity in fat tissue on in-body microwave propagation," in *Proc. IEEE Int. Microw. Biomed. Conf. (IMBioC)*, Jun. 2018, pp. 136–138.

[9] N. B. Asan, E. Hassan, M. D. Perez, S. R. M. Shah, J. Velander, T. J. Blokhuis, T. Voigt, and R. Augustine, "Assessment of blood vessel effect on fat-intrabody communication using numerical and ex-vivo models at 2.45 GHz," *IEEE Access*, vol. 7, pp. 89886–89900, 2019.

[10] N. B. Asan, C. P. Penichet, S. R. M. Shah, D. Noreland, E. Hassan, A. Rydberg, T. J. Blokhuis, T. Voigt, and R. Augustine, "Data packet transmission through fat tissue for wireless intrabody networks," *IEEE J. Electromagn., RF Microw. Med. Biol.*, vol. 1, no. 2, pp. 43–51, Dec. 2017.

[11] W. Emerson, "Electromagnetic wave absorbers and anechoic chambers through the years," *IEEE Trans. Antennas Propag.*, vol. AP-21, no. 4, pp. 484–490, Jul. 1973.

[12] A. Farahbakhsh, M. Khalaj-Amirhosseini, and H. Oraizi, "Ellipsoid anechoic chamber for radiation pattern measurments," in *Proc. IEEE 15th Medit. Microw. Symp. (MMS)*, Nov. 2015, pp. 1–3.

[13] A. Farahbakhsh and M. Khalaj-Amirhosseini, "Using metallic ellipsoid anechoic chamber to reduce the absorber usage," *IEEE Trans. Antennas Propag.*, vol. 63, no. 9, pp. 4229–4232, Sep. 2015.

[14] L. H. Hemming, *Electromagnetic Anechoic Chambers: A Fundamental Design and Specification Guide*. Hoboken, NJ, USA: Wiley, 2002.

[15] Q. Xu and Y. Huang, *Anechoic and Reverberation Chambers: Theory, Design, and Measurements*. Hoboken, NJ, USA: Wiley, 2019.

[16] I. Expósito, M. G. Sánchez, and I. Cuiñas, "Uncertainty assessment of a small rectangular anechoic chamber: From design to operation," *IEEE Trans. Antennas Propag.*, vol. 68, no. 6, pp. 4871–4880, Jun. 2020.

[17] T. Khalid, L. Albasha, N. Qaddoumi, and S. Yehia, "Feasibility study of using electrically conductive concrete for electromagnetic shielding applications as a substitute for carbon-laced polyurethane absorbers in anechoic chambers," *IEEE Trans. Antennas Propag.*, vol. 65, no. 5, pp. 2428–2435, May 2017.

[18] I. Munteanu and R. Kakerow, "Simulation methodology for the assessment of field uniformity in a large anechoic chamber," *IEEE Trans. Magn.*, vol. 50, no. 2, pp. 213–216, Feb. 2014.

[19] P. Suetens, *Fundamentals of Medical Imaging*, 3rd ed. Cambridge, U.K.: Cambridge Univ. Press, 2017.

[20] P. K. B. Rangaiah, J. Ebrahimizadeh, A. H. Nagaraju, I. El-Ali, M. Kouki, B. Mandal, F. Huss, M. D. Perez, and R. Augustine, "Clustering of dielectric and colour profiles of an ex-vivo burnt human skin sample," in *Proc. 14th Eur. Conf. Antennas Propag. (EuCAP)*, Mar. 2020, pp. 1–5.

[21] J. Engstrand, M. D. Perez, B. Mandal, J. Liden, C. Rohner, T. Voigt, and R. Augustine, "End-to-end transmission of physiological data from implanted devices to a cloud-enabled aggregator using fat intra-body communication in a live porcine model," in *Proc. 16th Eur. Conf. Antennas Propag. (EuCAP)*, Mar. 2022, pp. 1–5.

[22] D. M. Pozar, *Microwave Engineering*, 4th ed. Hoboken, NJ, USA: Wiley, 2012.

[23] *Acoustics—Determination of Sound Power Levels and Sound Energy Levels of Noise Sources Using Sound Pressure—Precision Methods for Anechoic Rooms and Hemi-Anechoic Rooms*, European Standard EN ISO 3745:2012(E), 2012.

[24] COMSOL. *Anechoic Chamber Absorbing Electromagnetic Waves*. Accessed: Mar. 22, 2023. [Online]. Available: https://www.comsol.com/model/anechoic-chamber-absorbing-electromagnetic-waves-38681

[25] A. Foley. (Jul. 9, 2014). *Modeling an RF Anechoic Chamber Using Periodic Structures, COMSOL Blog*. Accessed: Mar. 22, 2023. [Online]. Available: https://www.comsol.com/blogs/modeling-RF-anechoic-chamber-using-periodic-structures/

[26] C. A. Balanis, *Antenna Theory: Analysis and Design*, 4th ed. Hoboken, NJ, USA: Wiley, 2016.

[27] Leader Tech. *EA EMI Microwave Absorbers*. Accessed: Mar. 21, 2023. [Online]. Available: https://www.leadertechinc.com/assets/files/catalogs/absorbers.pdf

[28] P. Störchle, W. Müller, M. Sengeis, S. Lackner, S. Holasek, and A. Fürhapter-Rieger, "Measurement of mean subcutaneous fat thickness: Eight standardised ultrasound sites compared to 216 randomly selected sites," *Sci. Rep.*, vol. 8, no. 1, Nov. 2018, Art. no. 16268.

[29] L. Joseph, M. D. Perez, and R. Augustine, "Development of ultra-wideband 500 MHz–20 GHz human skin phantoms for various microwaves based biomedical applications," in *Proc. IEEE Conf. Antenna Meas. Appl. (CAMA)*, Sep. 2018, pp. 1–3.

[30] *Anechoic Chambers, Part 1: Shield Attenuation Measurement*, European Standard EN 50147-1:1996 E, 1996.

[31] Fei Teng Wireless Technology. *Model HA-07M18G-NF, 700 MHz to 18 GHz Double Ridged Broadband Waveguide Horn Antenna*. Accessed: Jan. 2, 2023. [Online]. Available: https://drive.google.com/file/d/1xQNXkyQQxt3MMc3FHCgo7L2IpTN1JNc7/view

[32] ETS Lindgren. *AMS-8800 Series Antenna Measurement System*. Accessed: Mar. 21, 2023. [Online]. Available: https://www.ets-lindgren.com/datasheet/chambers/wireless-test-systems/5008/500809

[33] Siretta. *Mike 1C 2G/3G/4G and WiFi Magnetic Stubby Antenna*. Accessed: Mar. 21, 2023. [Online]. Available: https://www.siretta.com/?smd_process_download=1&download_id=17304

[34] *Electromagnetic Compatibility (EMC)—Part 4–3: Testing and Measurement Techniques—Radiated, Radio-Frequency, Electromagnetic Field Immunity Test*, IEC Standard 61000-4-3:2006(E), 2006.

[35] Y. S. Meng, J. Deng, and Y. Shan, "Traceable site-VSWR measurements for validating anechoic chamber," in *Proc. Conf. Precis. Electromagn. Meas. (CPEM)*, Jul. 2018, pp. 1–2.

[36] *Specification for Radio Disturbance and Immunity Measuring Apparatus and Methods—Part 1–4: Radio Disturbance and Immunity Measuring Apparatus—Antennas and Test Sites for Radiated Disturbance Measurements*, IEC Standard CISPR 16-1-4:2019, 2019.

[37] A.H. Systems. *SAS-571 Double Ridge Guide Horn Antenna, 700 MHz–18 GHz*. Accessed: Mar. 21, 2023. [Online]. Available: https://www.ahsystems.com/datasheets/SAS-571_Horn_antenna_Datasheet.pdf

[38] B. Mandal, A. Chatterjee, P. Rangaiah, M. D. Perez, and R. Augustine, "A low profile button antenna with back radiation reduced by FSS," in *Proc. 14th Eur. Conf. Antennas Propag. (EuCAP)*, Mar. 2020, pp. 1–5.

PRAMOD K. B. RANGAIAH (Member, IEEE) received the B.E. degree in electronics and communication engineering from the Dr. Ambedkar Institute of Technology, Bengaluru, and the M.Tech. degree in RF communication and the Ph.D. degree in electronics engineering from Jain University, Bengaluru. Throughout his career, he has gained valuable industry experience, as an RF Design Trainee with Icon Design and Automation Pvt. Ltd., and conducting research as a Visiting Scholar with the University of Concordia, Montreal, QC, Canada. He is currently a Distinguished Researcher in the field of microwaves in medical engineering. He is also a Researcher with Ångström Laboratoriet, Uppsala University, Sweden, where he has made significant contributions to the field through his expertise and research endeavors. He has established himself as a Renowned Expert. His dedication to advancing the scientific community is evident through his membership in esteemed organizations, such as IEEE, ISTE, and IETE. His research interests include various aspects of microwaves in medical engineering, encompassing the design, characterization, and optimization of RF passive devices, board-level tuning, low-noise amplifiers, power amplifiers, circuit linearization, high-efficiency design techniques, and circuit instability strategies. His commitment to scholarly publishing is demonstrated by his role as an Associate Editor of *International Journal of Big Data Management* (Inderscience Publishers) and an Editorial Board Member of *Frontiers* and *International Journal of Advanced And Applied Sciences*. Furthermore, he actively contributes to the scientific community as a peer reviewer for prestigious international journals, including IEEE Access, MDPI, Inderscience Publishers, *Advances in Science, Technology and Engineering Systems Journal*, and *International Journal of Advance Research and Innovative Ideas in Education*.

ROGER L. KARLSSON received the M.Sc. degree in applied physics and the Ph.D. degree in space physics from Uppsala University, Uppsala, Sweden, in 1997 and 2005, respectively. In 2000, he co-founded the company Red Snake Radio Technology AB. From 2005 to 2006, he was with ScandiNova Systems AB, Uppsala. From 2006 to 2011, he was Postdoctoral Researcher with the Space Research Institute, Austrian Academy of Sciences, Graz, Austria. From 2008 to 2011, he was a Senior Lecturer with the Department of Physics and Astronomy, Uppsala University. From 2012 to 2023, he was with ScandiNova Systems AB, which produces pulse modulators for pulsed high-power klystrons and magnetrons and also complete RF units, which outputs high-power (MW) microwaves. At ScandiNova Systems AB, he was responsible for RF, including design and test of both low-level and high-power RF-systems, extending to complete customized waveguide systems, both pressurized and for ultra-high vacuum. Since 2018, he has been a Senior Researcher with the Department of Electrical Engineering, Division of Solid State Electronic, Microwave in Medical Engineering Group, Uppsala University, where he is involved in research and teaching. His main research interests include microwave engineering and antennas.

ARVIND SELVAN CHEZHIAN is currently pursuing the Ph.D. degree in medical robotics and biomechatronics with the Department of Electrical Engineering, Division of Solid State Electronics, Uppsala University. He delves into concepts, such as bionic arms, exoskeletons, and medical robots, leveraging his knowledge of IBC and advanced fabrication techniques. His ultimate goal is to develop cutting-edge medical technologies that seamlessly integrate with the human body, enhancing mobility, rehabilitation, and prosthetics. His multidisciplinary approach and unwavering commitment to advancing technology in the biomedical field position him as a promising researcher in healthcare innovation. With his work, he aims to contribute to developing next-generation medical solutions that will revolutionize patient care and improve quality of life. His research interest includes phantom fabrication for IBC applications, specifically modeling tissues like fat, muscle, skin, and bone. His expertise extends beyond his core research, including 3D-printed prototypes for biomedical applications, microwave sensor testing, and PCB fabrication.

LAYA JOSEPH received the engineering degree in electronics and communication from Calicut University, India, in 2009, and the master's degree in engineering physics from Uppsala University, Sweden, in 2019, where she is currently pursuing the Ph.D. degree with the Microwaves in Medical Engineering Group (MMG), Division of Solid-State Electronics, Department of Electrical Engineering, Ångström Laboratoriet. From 2019 to 2021, she was a Research Engineer with Ångström Laboratoriet, Division of Solid State Electronics, MMG, Uppsala University. In 2020, she was a Research Engineer with the Micro Structure Technology (MST), Material Science Department. Her research interests include biological microwave phantoms for intra-body communication, fat intra-body communication, breast tumor sensing, and stretchable printed circuit boards for skin worn wireless networks.

BAPPADITYA MANDAL (Member, IEEE) was born in India, in 1985. He received the B.Tech. degree in electronics and communication engineering from the Kalyani Government Engineering College, Maulana Abul Kalam Azad University of Technology (Formerly WBUT), West Bengal, in 2008, and the M.E. degree in advanced communication and networking and the Ph.D. degree in microwave and antenna engineering from the Indian Institute of Engineering Science and Technology (IIEST), Shibpur, India, in 2010 and 2018, respectively. He is currently a Researcher with the Division of Solid-State Electronics, Microwaves in Medical Engineering Group (MMG), Department of Electrical Engineering, Ångström Laboratory, Uppsala University (UU), Sweden. His current research interests include wearable antennas implantable antenna and non-invasive microwave sensors for biomedical applications. He has served as a Regular Reviewer for various prestigious SCI journals, such as IET *Electronics Letters*, IEEE TRANSACTIONS ON ANTENNAS AND PROPAGATION, and RFCAD.

BOBINS AUGUSTINE (Member, IEEE) received the B.Sc. degree in physics from Mahatma Gandhi University, Kottayam, India, in 2008, the master's degree in applied physics from the Cochin University of Science and Technology (CUSAT), India, in 2010, and the D.Sc.Tech. degree from the University of Oulu, Finland, in 2016. After a Project Fellow with CUSAT, he received the Nordic Scholarship to do his doctorate in printed electronics with the University of Oulu, in 2011. Since then, he has been a Postdoctoral Researcher and a Specialist in the field of printed electronics. Since 2019, he has been a Visiting Researcher with Linköping University, Sweden. He is currently a Researcher with Uppsala University, Sweden, and the Uppsala Networked Objects (UNO)/Department of Information Technology and the Microwaves in Medical Engineering Group (MMG)/Department of Electrical Engineering. He was also a part of many renowned Finnish projects funded by HILLA and Business Finland (Tekes). His research interests include flexible printed electronic devices, such as sensors, antennas, OLEDs, solar cells, OTFTs, conducting polymers/transparent conducting oxides, and soft robotics and actuators. In the beginning of 2021, he won the prestigious and highly competitive Marie Skłodowska Curie Fellowship-H2020 IF from EU Research Executive Agency for his project proposal titled Soft Amphibious Micro Robots fabricated by Additive Integrated manufacturing (SAMURAI) and it is intended for in-vivo micro robotic surgery and drug delivery.

MARIA MANI received the M.D. degree from Lund University, in 2001, and the Ph.D. degree from Uppsala University, Uppsala, Sweden, in 2010. She is currently a Senior Consultant and the Director of microsurgery and the Chief of Doctors with the Department of Plastic and Reconstructive Surgery, Uppsala University Hospital. She is also a specialist trained as a plastic surgeon in Uppsala in addition to two years of microsurgical fellowships in London. As an Associate Professor and an Adjunct Lecturer with Uppsala University, she mentors a number of Ph.D. and research students. Her clinical work includes advanced microsurgical procedures for complex cancer and post-traumatic wounds and defects. Her current research interests include breast cancer, lymphedema, and translational pre-clinical collaborations.

MAURICIO DAVID PEREZ (Member, IEEE) was born in Buenos Aires, Argentina, in 1980. He received the engineering degree in electronics from National Technological University (UTN), Argentina, in 2007, and the Ph.D. degree in electrical engineering from the University of Bologna (UNIBO), Italy, in 2012. From 2012 to 2014, he was an Industrial Researcher in Italy. From 2014 to 2017, he was an Academic Teacher and Researcher with UTN. He is currently a Teacher and a Researcher with Ångström Laboratories, Microwaves in Medical Engineering Group (MMG), Uppsala University (UU), Sweden. His current research interest includes modeling and data-driven validation of microwave sensors for biomedical applications.

THIEMO VOIGT (Member, IEEE) received the Ph.D. degree from Uppsala University, Sweden, in 2002. He is currently a Professor of computer science with the Department of Information Technology, Uppsala University. He also leads the Networked Embedded Systems Group, RISE Computer Science. His work has been cited more than 18,700 times. His current research interests include system software for embedded networked devices and the Internet of Things. He is a member of the editorial board for the IEEE Internet of Things and *ACM Transactions on Sensor Networks* (TOSN).

ROBIN AUGUSTINE (Member, IEEE) received the degree in electronics science from Mahatma Gandhi University, India, in 2003, the master's degree in electronics with robotics specialization from the Cochin University of Science and Technology, India, in 2005, and the Ph.D. degree in electronics and optic systems from the Univerisité Paris-Est Marne-La-Vallée, France, in July 2009. He was a Postdoctoral Researcher at the University of Rennes 1, Brittany, France, from 2009 to 2011. In 2011, he joined Uppsala University as a Senior Researcher, where he became an Associate Professor, in February 2016. He is currently a Senior University Lecturer in medical engineering and a Docent in microwave technology. He is also the Head of the Microwaves in Medical Engineering Group (MMG), Uppsala University, and the Founder, the Chairperson, and the CTO of Probingon AB, Swedish Medtech Company. He was a part of Vinnova Project on skin cancer diagnostic tool based on micromachined interface for high-resolution THz spectroscopy (MTSSC). He is a Co-PI of the EU Project SINTEC, SSF framework grant LifeSec, Vinnova grant connect my body, in 2018, and the SSF framework grant Zero-IoT 2020, the Research Lead of the Eurostars Project SenseBurn 2018, and the Project Leader of Eurostars Project MAS 2020. He is also an EU Coordinator of HORIZON 2020 FET-OPEN Science Excellence Project B-CRATOS, a visionary project in man machine interface. He has been invited at the Swedish Royal Academy of Sciences to present his work on noninvasive physiological sensing. He is also a Project Coordinator for Indo-Swedish Vinnova Project BDAS and Swedish part of the bilateral (The Netherlands and Sweden) Horizon 2020 Eurostars Project COMFORT. He is the author or coauthor of more than 180 publications, including journals and conferences and has three patents. His thesis topic was "Electromagnetic modeling of human tissues and its application on the interaction between antenna and human body in the BAN context." Two Ph.D. students graduated in 2019 under his supervision. He has received Carl Trygger and Olle Engqvist fundings for his postdoctoral research. His current research interests include designing of wearable antennas, BMD sensors, microwave phantoms, dielectric characterization, bionics, mechatronics, non-invasive diagnostics, point of care sensors for physiological monitoring, clinical trials, animal trials, and on body microwave communication. He has pioneered the Fat—Intra Body Communication Technique. He was a recipient of UGCRFSMS fellowship from Indian Government and EGIDE Eiffel grant for excellence from French Research Ministry, in 2006 and 2008, respectively, and the Swedish Research Agency, Vetenskapsrådet's (VR) Project grant 2017 for his project on "A Novel Modality for Osteodiagnosis" and the Attractive Innovation Project 2020 Award from Uppsala University Innovation. He is the Regular Sessions Chair and a Convened Session Organizer of EuCAP. He is an Editorial Board Member of IET *Electronics Letters* and *Frontiers in Communication*. He has been a Board Member of the Department of Electrical Engineering, since January 2020.